MATERIALS SCIENCE

# Role of hierarchy structure on the mechanical adaptation of self-healing hydrogels under cyclic stretching

**Xueyu Li[1], Kunpeng Cui[2,3], Yong Zheng[2], Ya Nan Ye[1,4], Chengtao Yu[5,6], Wenqi Yang[5], Tasuku Nakajima[1,2], Jian Ping Gong[1,2]***



**Soft materials with mechanical adaptability have substantial potential for various applications in tissue engineering. Gaining a deep understanding of the structural evolution and adaptation dynamics of soft materials subjected to cyclic stretching gives insight into developing mechanically adaptive materials. Here, we investigate the effect of hierarchy structure on the mechanical adaptation of self-healing hydrogels under cyclic stretching training. A polyampholyte hydrogel, composed of hierarchical structures including ionic bonds, transient and permanent polymer networks, and bicontinuous hard/soft-phase networks, is adopted as a model. Conditions for effective training, mild overtraining, and fatal overtraining are demonstrated in soft materials. We further reveal that mesoscale hard/soft-phase networks dominate the long-term memory effect of training and play a crucial role in the asymmetric dynamics of compliance changes and the symmetric dynamics of hydrogel shape evolution. Our findings provide insights into the design of hierarchical structures for adaptive soft materials.**

## INTRODUCTION

Cyclic stretching is an effective physical exercise for humans that increases muscle and tendon compliance with deformations (*1*). The training effect proves optimal at an appropriate stretching magnitude and repetition periods and diminishes after rest owing to detraining (*2*, *3*). Overtraining, on the other hand, which occurs at extreme exercise and overly long training periods, damages biotissues (*4*, *5*). Synthetic hydrogels, which combine cross-linked polymer as solid and water as liquid components, have similarities to soft tissues in the human body and hold substantial potential for applications as artificial tissues to replace damaged ones (*6*). These applications require hydrogel to exhibit mechanical adaptability, such as effective training, detraining, and overtraining, in response to long-term mechanical stimuli. However, reports on such mechanical adaptation over a wide range of deformations are rare.

Researchers have recently proposed strategies that mimic the adaptation of muscles to mechanical stimuli using chemical and mechanical mechanisms in hydrogels. A self-growing double-network (DN) system based on force-triggered polymerization in DN hydrogels is one example of a chemical mechanism (*7*, *8*). It is an open system resembling metabolic processes in the human body in which monomers can diffuse into DN hydrogels to reconstruct a damaged network induced by mechanoradicals. In this system, mechanical training triggers irreversible changes in the network structure, consequently affecting its mechanical performance. As the training cycles increase, a transition from soft and ductile materials to hard and brittle materials occurs due to an increase in polymer density and a reduction in water content. Owing to the complexity of the human body, creating synthetic hydrogels with bio-tissue–like mechanical adaptability is still a challenge. Mechanically induced nanofiber and nanocrystallization systems are examples of physical mechanisms (*9*–*11*). Although they are closed systems that do not exchange substances with their surroundings, the mechanical adaptation phenomena occurred during cyclic stretching of synthetic hydrogels, such as shakedown (*12*–*14*), fatigue (*14*–*23*), and self-recover (*24*–*30*), also occur in muscles and tendons during daily activities like walking, running, throwing, climbing, and lifting heavy loads. However, there is a lack of understanding regarding the effects of cyclic stretching on the structural evolution and correlated dynamics of mechanical adaptation in synthetic hydrogels, especially those with hierarchical structures. Furthermore, the reasons behind the substantial reduction in stretchability of tough hydrogels under cyclic stretching, in contrast to typical high extensibility under monotonic stretching (*13*), remain poorly understood.

We investigated physical mechanisms behind cyclic stretching (referred to as training) and rest in a strain-free state (referred to as detraining) and the training effect on fatigue resistance in hydrogels. Self-healing hydrogels with dynamic bonds are potential materials to exhibit dynamic training effects in closed systems. However, most self-healing hydrogels, such as dually cross-linked gels (*31*–*35*), dynamically cross-linked homogeneous poly(ethylene glycol) network gels (*36*–*38*), and host-guest gels (*39*–*41*), have relatively simple network structures. Relaxation dynamics depend on collective diffusion of polymer network and the dissociation rate of their reversible transient networks, resulting in relaxation time shorter than 1 s (*35*). It probably endows a negligible memory effect during mechanical training. This is in contrast to muscles and tendons, which have an elaborate hierarchical structure that

[1]Laboratory of Soft and Wet Matter, Faculty of Advanced Life Science, Hokkaido University, Sapporo 001-0021, Japan. [2]Institute for Chemical Reaction Design and Discovery (WPI-ICReDD), Hokkaido University, Sapporo 001-0021, Japan. [3]Department of Polymer Science and Engineering, University of Science and Technology of China, Hefei 230026, China. [4]College of Materials Science and Engineering, Taiyuan University of Technology, Taiyuan 030024, China. [5]Laboratory of Soft and Wet Matter, Division of Soft Matter, Graduate School of Life Science, Hokkaido University, Sapporo 060-0810, Japan. [6]Institute of Zhejiang University-Quzhou, Quzhou 324000, China.
*Corresponding author. Email: gong@sci.hokudai.ac.jp

is able to adapt to mechanical training and contribute long-term retention of mechanical training effects with the aid of physiological processes (*42*, *43*). The question is whether the hierarchical structures themselves contribute to the long-term memory to the training effect and what role is played by hierarchical structure in the mechanical adaptation during training, detraining, and overtraining. Here, we apply cyclic mechanical deformation to self-healing hydrogels with hierarchical structures. By combining small-angle x-ray scattering (SAXS) measurements, viscoelastic model fitting, and fatigue tests of trained samples, we identify the underlying mechanisms of training and their relation to multiscale structures. We demonstrate that mesoscale hard/soft-phase networks contribute to fracture resistance under cyclic stretching at substantially high deformations, and they govern the long-term memory effect of training. In addition, the hard/soft-phase networks also play a crucial role in the asymmetric dynamics of compliance changes and in the symmetric dynamics of hydrogel shape evolution under strain. The current work provides a useful step toward elucidating the essential physics governing long-term memory in response to cyclic mechanical training in soft materials with hierarchical structures.

### The material and experimental design

We adopted a tough polyampholyte (PA) hydrogel (*44*), which was prepared by random copolymerization of oppositely charged ionic monomers consisting of sodium *p*-styrenesulfonate (NaSS) and methyl chloride quarternized *N*,*N*-dimethylamino ethylacrylate (DMAEA-Q), as a model material. In this study, unless otherwise specified, we primarily utilized the strongly phase-separated PA (s-PA) gel, which has high modulus contrast between the hard- and soft-phase networks. The s-PA gel has hierarchical structures consisting of ~1-nm transient network by dynamic ionic bonds, ~10-nm permanent polymer network by trapped entanglement and chemical cross-linking, and ~100-nm bicontinuous hard/soft-phase networks by microphase separation (Fig. 1A and fig. S1). Bicontinuous hard/soft-phase networks are driven by Coulombic and hydrophobic interactions on the PA chains. Ionic bonds offer self-healing properties. Hierarchical structures impart multiscale structural change and time responses to repetitive mechanical stimuli.

The s-PA gel exhibited sticky Rouse-like relaxation in the dynamic mechanical spectra (*45*–*47*). The stickers (ionic bonds), which are the building blocks of the hierarchical structure, have a short lifetime $\tau_s < 10^{-5}$ $s^{-1}$ (fig. S2). The hard-phase network, which has denser polymers and stickers, has more restricted mobility (*48*), leading to a longer relaxation time than the soft-phase network. The in situ SAXS reveals that the maximum stretch ratio $\lambda_{affine}$ for the affine deformation of bicontinuous phase networks, corresponding to the onset of damage to the hard-phase network, is $\lambda_{affine} = 3.06$, while the maximum stretch ratio $\lambda_c$ for the onset of damage to the soft-phase network is $\lambda_c = 9.2$ (fig. S1). Bicontinuous hard- and soft-phase networks endow the s-PA gels with high toughness and strong fatigue resistance (*47*, *49*, *50*) via multiscale energy dissipation mechanisms under uniaxial monotonic stretching (*51*): (i) At a stretch ratio $\lambda < \lambda_{affine}$, the percolated two-phase networks deform affinely, but the hard-phase network sustains more stress due to high stiffness. Meanwhile, the nanoscale chain conformation elongates with ionic bonds breaking to dissipate energy. (ii) At $\lambda_{affine} < \lambda < \lambda_c$, deformation of the percolated hard- and soft-phase network deviates from affine deformation. The hard-phase network strands damage as they carry most of the stress, and the contraction of the damaged hard-phase strands exerts a large shear stress on the adjacent soft-phase strands. The load is transferred to adjacent hard-phase strands via soft-phase strands. (iii) At $\lambda > \lambda_c$, most of the hard-phase strands rupture, and the shear stress increases to larger than the strength of soft-phase network. This results in rupture of soft-phase network and global failure of the gel. Because the soft-phase network has a shorter relaxation time than the hard-phase network, s-PA gels exhibit intriguing cyclic loading behavior: The shape of the gel recovers faster than its compliance recovers (*51*) in a similar manner to muscles and tendons (*52*, *53*). This contrasts with self-healing materials with no hierarchical structure, which exhibit simultaneous recovery of shape and compliance (*26*, *31*). These behaviors reinforce the idea that s-PA hydrogels are highly suitable for studying dynamic training and detraining behaviors.

Here, we applied successive cyclic loading to the s-PA gels with stretching ratios $\lambda_{tr}$ below and above $\lambda_{affine}$ to clarify their relation to training, detraining, and overtraining. We found that $\lambda_{tr}$ plays a critical role in multiscale structural evolution. For $\lambda_{tr} < \lambda_{affine}$, bicontinuous phase networks remain intact, and cyclic training mainly elongates those networks by breaking and re-bonding the rearranged ionic bonds (Fig. 1B) (*49*). This caused a decrease in the strain energy needed for a specific deformation ($W_d$) until the breaking and re-bonding of ionic bonds (as well as the orientation of the bicontinuous phase networks) gradually reached the steady state, resulting in a plateau in $W_d$ (training process). During the rest period in a strain-free state, the polymer network's entropy elasticity facilitated a rapid initial recovery of $W_d$ at the beginning. However, owing to the slow dynamics of the hard-phase network, the $W_d$ returned to the level initially required for the pristine sample requires elongated time (detraining process), as shown in Fig. 1C. Because the phase networks form a relatively stable or higher oriented structure during cyclic training, the recovery rate of $W_d$ slows down with extended duration ($t_{tr}$) or increased training intensity. For $\lambda_{affine} < \lambda_{tr} < \lambda_c$, damage to the hard-phase network occurred, whereas the soft-phase network remained intact (Fig. 1B). Damage to the hard-phase network that accumulated with cyclic loads showed an irreversible overtraining effect (Fig. 1C). For $\lambda_{tr} \approx \lambda_c$, the gel cannot sustain long-time cyclic training because most of the hard-phase strands rupture, leading to shear stress exceeding the strength of the soft-phase network. Consequently, the gel fractures within dozens of cycles. Therefore, this study mainly focuses on the cyclic training behaviors at $\lambda_{tr} < \lambda_c$.

## RESULTS

### Training and detraining through cyclic loading and resting

The s-PA gel training experiments were performed using an unnotched sample having a pure shear geometry (Fig. 2A). Cyclic training was conducted continuously for $N_{tr} = 10^4$ cycles at a nominal strain rate of 1 $s^{-1}$ without intervals between cycles. Maximum and minimum stretch ratios were maintained at preset values $\lambda_{tr}$ and 1, respectively. The preset $\lambda_{tr}$ ranged from $\lambda_{tr} = 1.7$ to 7.1, covering both $\lambda_{tr} < \lambda_{affine}$ and $\lambda_{affine} < \lambda_{tr} < \lambda_c$ regimes, unless otherwise specified. After resting for $t_{rest}$, trained gels were reloaded to their corresponding $\lambda_{tr}$ to determine their recovery efficiency. The longest $t_{rest}$ that we tracked was 87 ks for $\lambda_{tr} < 4.1$ and 500 ks for $\lambda_{tr} > 4.1$ (1 ks equals 1000 s). All cyclic training and

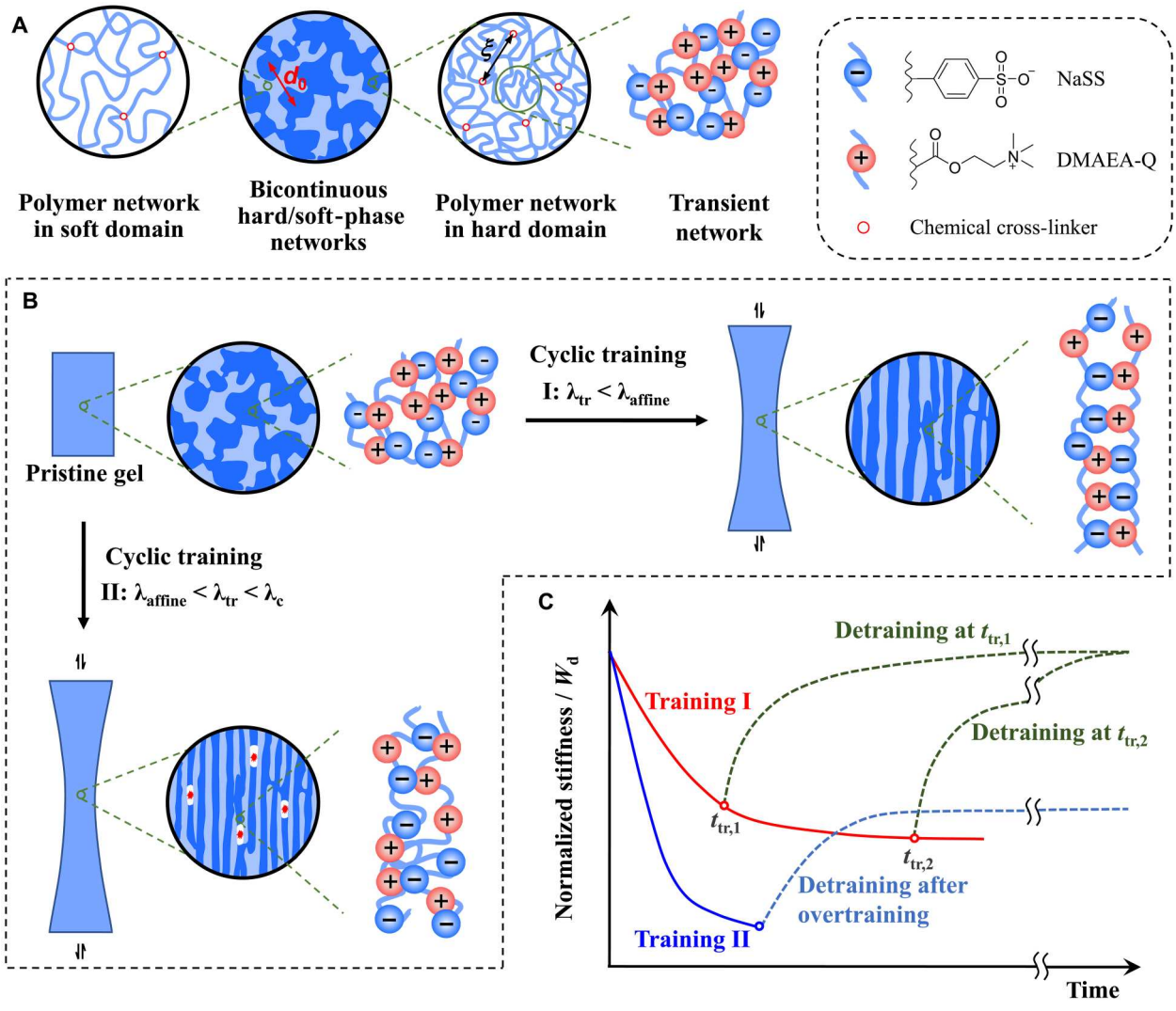


**Fig. 1. Schematic illustrations of hierarchical structures in s-PA gel and their dynamic adaptation to mechanical training.** (**A**) Multiscale structure in s-PA gel, including ~1-nm transient network by dynamic ionic bonds, ~10-nm (mesh size ξ) permanent polymer network by entanglement and cross-linking, and ~100-nm (*d*-spacing $d_0$) bicontinuous hard/soft-phase networks by phase separation. The gel has at least three relaxation times related to the three networks (the transient network, the soft-phase network, and the hard-phase network). They are accumulations of ionic aggregations. (**B**) A scheme of the deformation of bicontinuous phase networks and transient network to cyclic training at conditions (I) $\lambda_{tr} < \lambda_{affine}$ and (II) $\lambda_{affine} < \lambda_{tr} < \lambda_c$. I: Both the hard- and soft-phase networks are intact. II: Damage occurs in the hard-phase network, while the soft-phase network remains intact. $\lambda_{affine}$ and $\lambda_c$ are maximum stretch ratio for the onset for the damage of the hard- and soft-phase networks, respectively (fig. S1). (**C**) A scheme of effective training (Training I), overtraining (Training II), and detraining. Under successive cyclic training stimuli, a stretch-induced decrease of stiffness and strain energy to a specific deformation ($W_d$) that increased compliance of the material (red curve). For Training I, the stiffness and $W_d$ recover during detraining (dashed green curves). The recovery rate depends on duration ($t_{tr}$) and training intensity. Overtraining occurred during Training II causing unrecoverable damage.

resting experiments were performed at 24°C in a humidity chamber. Water vapor was sustainably supplied to the chamber during the test to prevent sample dehydration.

Figure 2B shows the evolution of the loading-unloading curves with training cycle $N_{tr}$ at $\lambda_{tr} = 3.7$. Vigorous softening with a large residual stretch ratio ($\lambda_{res}$) was observed before $N_{tr} \approx 1000$ cycles, followed by little change in loading-unloading curves. This phenomenon is known in mechanics as a shakedown (*12*, *54*). Figure 2C shows that loading-unloading curves gradually recover with resting time $t_{rest}$ after the gel was trained at $\lambda_{tr} = 3.7$ for $N_{tr} = 10^4$ cycles. We adopted two parameters, energy required for a specific deformation [work of extension ($W_{ex}$)] and residual stretch ratio ($\lambda_{res}$) (Fig. 2D), to quantify the compliance changes and hydrogel shape evolutions, respectively, in the training and detraining processes. Figure 2E shows an example of evolution of the two parameters with training and detraining time. The normalized $W_{ex}/W_{ex0}$ (where $W_{ex0}$ is the work of extension of the first loading) drops sharply at the beginning of training, due to the elongation of polymer network with massive ionic bonds breaking. Then, $W_{ex}/W_{ex0}$ decreases slightly with a further increase in training time (orange regime). $W_{ex}/W_{ex0}$ recovers rapidly at the beginning of rest (detraining) and gradually approaches 0.8 with extended

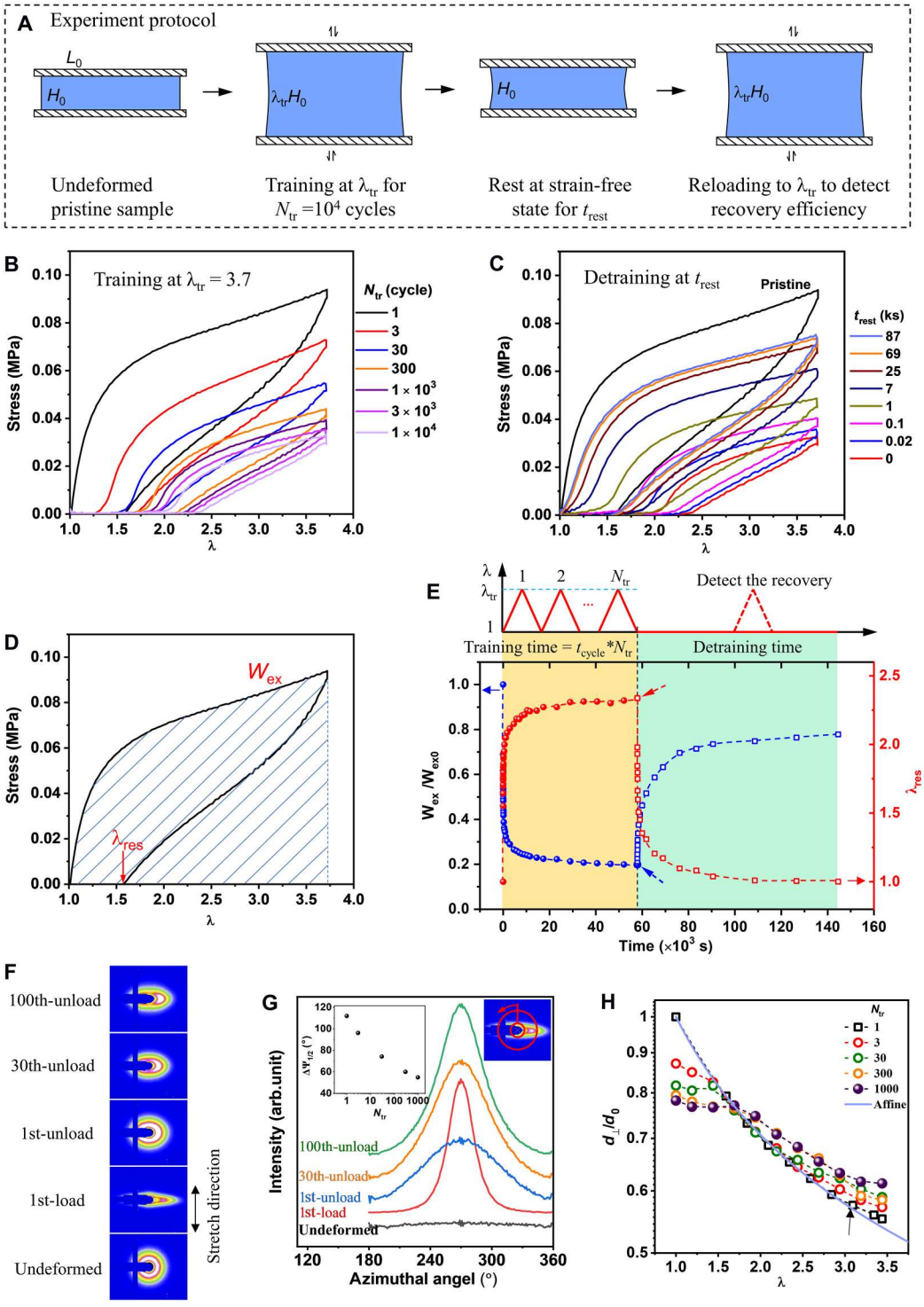


**Fig. 2. Cyclic training of s-PA gel and evolution of the bicontinuous phase structure.** (**A**) Experimental protocol for cyclic training and detraining (rest). $L_0$ = 50 mm, $H_0$ = 10 mm, and $\lambda_{tr}$ = 1.7 to 7.1. (**B**) Evolution of loading-unloading curves with training cycle ($N_{tr}$). (**C**) Loading-unloading curves for a trained gel resting for $t_{rest}$. Training at $\lambda_{tr}$ = 3.7 for $N_{tr}$ = 10$^4$ cycles is taken as an example. (**D**) Scheme for work of extension ($W_{ex}$, total hatched area) and the residual stretch ratio ($\lambda_{res}$). (**E**) Normalized $W_{ex}/W_{ex0}$ and $\lambda_{res}$ in cyclic training and detraining as a function of time. Dashed arrows indicate the start point of detraining. The top scheme shows the corresponding training and detraining processes. Training at $\lambda_{tr}$ = 3.7 for $N_{tr}$ = 10$^4$ is taken as an example. (**F** and **G**) Cyclic training-induced evolution of 2D SAXS patterns (F) and the corresponding 1D azimuthal scan profiles (G). The right inset in (G) shows the azimuthal scan's integration $q$ range (between two concentric circles). The left inset shows the evolution of full peak width at half maximum ($\Delta\Psi_{1/2}$) of unloading sample (strain-free state) as a function of training cycle $N_{tr}$. $\lambda_{tr}$ = 2.9 < $\lambda_{affine}$ is taken as an example. (**H**) Microscopic deformation ($d_\perp/d_0$) in perpendicular to loading direction versus macroscopic stretch ratio λ for loading to different cycle number $N_{tr}$ at $\lambda_{tr}$ = 3.44. The $d_\perp/d_0$ decreases with λ, due to lateral contraction of phase network when elongation along the stretch direction (*51*). The blue line stands for the prediction of affine deformation ($d_\perp/d_0 = \lambda^{-1/2}$) of the phase networks perpendicular to the loading direction (incompressible materials). The black arrow indicates the maximum λ to show affine deformation of the bicontinuous hard/soft-phase networks ($\lambda_{affine} \approx 3.06$).

detraining time (green regime). $\lambda_{res}$ shows a trend opposite to that of $W_{ex}/W_{ex0}$. The final plateau of $W_{ex}/W_{ex0}$ in detraining does not recover to 1.0 within our observation time, whereas $\lambda_{res}$ recovers to 1.0, indicating that the gel shape recovers faster than its compliance.

Structural evolution during cyclic training was tracked by in situ SAXS (fig. S1). The two-dimensional (2D) SAXS pattern of the undeformed sample shows an isotropic ring (Fig. 2F). The 1D azimuthal scan profile shows no peaks (Fig. 2G), demonstrating an isotropic distribution of hard and soft domains in bicontinuous phase networks. When the sample was loaded to $\lambda_{tr}$ = 2.9, the 2D SAXS pattern converts to an elongated spot in the horizontal direction (Fig. 2F, 1st-load) and recovers to an ellipse when unloading to λ = 1 (Fig. 2F, 1st-unload). Meanwhile, the 1D azimuthal scan

profile changes from a narrow sharp peak for 1st-load to a broad peak for 1st-unload (*N*th-load and *N*th-unload indicate that the sample was measured when loading to $\lambda = \lambda_{tr}$ and unloading to $\lambda = 1$, respectively, at the *N*th cycle). In addition, the full peak width at half maximum ($\Delta\Psi_{1/2}$) of the 1D azimuthal scan profile increases from $\Delta\Psi_{1/2} = 28.1$ for 1st-load to $\Delta\Psi_{1/2} = 111.9$ for 1st-unload during the unloading process ($\Delta\Psi_{1/2} = 180°$ indicates an isotropic distribution of bicontinuous phase networks and $\Delta\Psi_{1/2} = 0°$ indicates a perfectly anisotropic distribution). These results demonstrate that the bicontinuous phase networks deform into a highly anisotropic structure under loading with the breaking and reforming of migrated ionic bonds on the elongated transient network (*51*) but mostly recover during the first unloading cycle. As the training cycle increased, the 1D azimuthal scan profiles of the unloaded sample narrows, and the corresponding $\Delta\Psi_{1/2}$ decreases with the cycle number, as shown in Fig. 2G. This suggests that an anisotropic structure can be retained better with more training cycles, coinciding with an increase in $\lambda_{res}$. In such a case, $\lambda_{tr} < \lambda_{affine}$, and the deformation of the phase network always obeys affine deformation, except for the $\lambda_{res}$ part (*49*). Orientation structures gradually adapted to consecutive cyclic training without damaging the bicontinuous phase network. However, during cyclic training at $\lambda_{affine} < \lambda_{tr} < \lambda_c$, non-affine deformation occurs from the very first cycle, and microscopic deformation ($d_\perp/d_0$) perpendicular to the loading direction increases with the number of cycles (Fig. 2H), indicating that damage accumulated in the hard-phase network (*49*, *51*).

### Effect of hierarchical structure on cyclic training behavior

To find the role of the hierarchical structure on the cyclic training behavior of s-PA gel, we further conducted cyclic training on two other soft self-healing materials. One is a PA gel with very weak-phase contrast (w-PA) as shown in fig. S3A; another is a viscoelastic elastomer without phase-separation structure (section S1). In the case of w-PA, although the fracture stretch ratio [$\lambda_f$ (monotonic)] under monotonic stretching is relatively high [$\lambda_f$ (monotonic) = 4.76], the gel only endured cyclic training for $N_{tr} = 10^4$ cycles at $\lambda_{tr} = 1.3$, and it fractured within thousands of training cycles at $\lambda_{tr} = 1.6$ (fig. S3C). This is in strong contrast to the s-PA gel that sustained cyclic training for $N_{tr} = 10^4$ cycles even at a very high stretch ratio of $\lambda_{tr} = 8.5$ (fig. S3E). The s-PA gel eventually fractured at $\lambda_{tr} = 9.1$ that is close to $\lambda_c$, the onset of damage to the soft-phase network during monotonic stretching (fig. S3, D and F). Considering the difference in polymerization degree of effective polymer strands ($N_{eff}$) in the two gels, here, we compare the ratio $\lambda_f$(cyclic)/$\lambda_f$(monotonic) to characterize the fracture resistance of cyclic stretching for different gels, where $\lambda_f$(cyclic) is the $\lambda_{tr}$ leading to sample fracture during cyclic training. We observed a high value of $\lambda_f$(cyclic)/$\lambda_f$(monotonic) = 0.95 for the s-PA gel and a low value of $\lambda_f$(cyclic)/$\lambda_f$(monotonic) = 0.34 for the w-PA gel (Table 1). These findings indicate that bicontinuous phase separation with strong modulus contrast may play a pivotal role in fracture resistance under cyclic stretching.

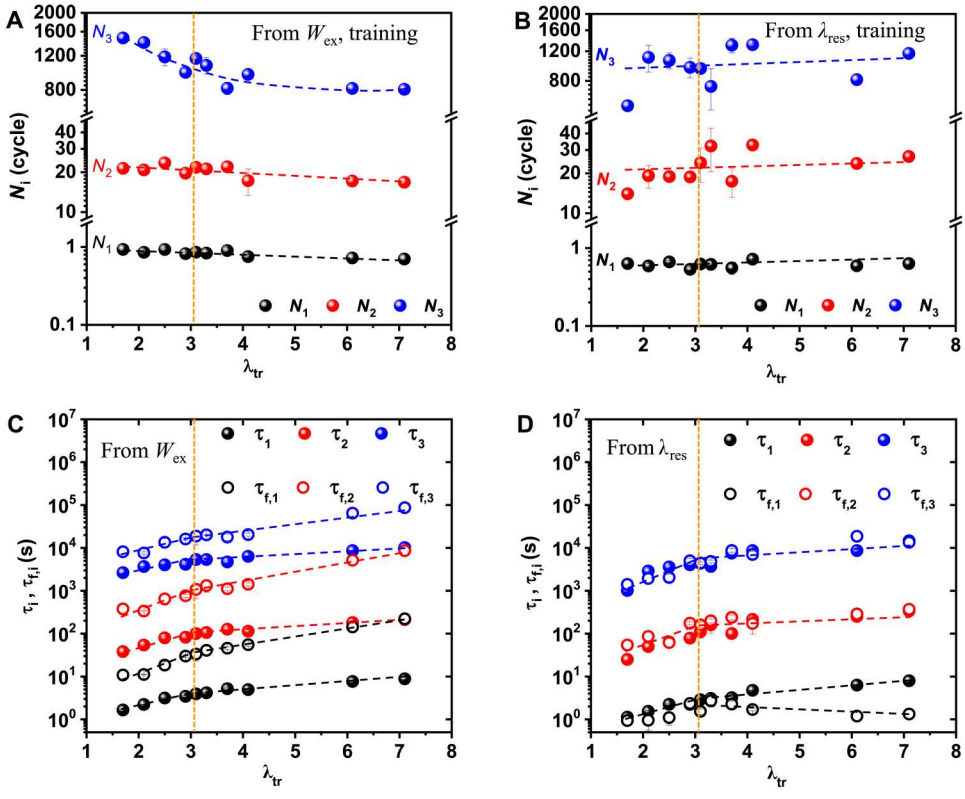


**Fig. 3. Characteristic training cycles and detraining times of s-PA gel at varied $\lambda_{tr}$ for $N_{tr} = 10^4$ cycles.** Characteristic training cycles and characteristic detraining times were obtained from the three-term Prony series fitting (see the Supplementary Materials). (**A** and **B**) Characteristic training cycles $N_1$, $N_2$, and $N_3$ of $W_{ex}$ (A) and $\lambda_{res}$ (B) as a function of $\lambda_{tr}$. (**C** and **D**) Characteristic training time $\tau_i$ and characteristic detraining time $\tau_{f,i}$ versus $\lambda_{tr}$ for $W_{ex}$ (C) and $\lambda_{res}$ (D). The vertical dashed line indicates $\lambda_{affine}$. Dashed lines are guides for the eyes. The error bar ($\lambda_{tr}$ = 2.1 to 3.7) is SE from at least three measurements.

**Table 1. Comparison of the fracture stretch ratio of s-PA and w-PA gels and non-phase-separated PPEA elastomer under monotonic and cyclic stretching.** s-PA, strongly phase-separated PA; w-PA, weakly phase-separated PA; PPEA, poly(ethylene glycol phenyl ether acrylate).

| Material | Phase separation | Plateau modulus (kPa) | $N_{eff}$* | $\lambda_f$ (monotonic) | $\lambda_f$ (cyclic) | $\lambda_{max}$† | $\lambda_f$ (cyclic)/$\lambda_f$ (monotonic) |
|---|---|---|---|---|---|---|---|
| s-PA gel | Strong | 112.7 | 986 | 9.57 ± 0.14 | 9.1 | 8.5 | 0.95 |
| w-PA gel | Weak | 287.4 | 378 | 4.76 ± 0.14 | 1.6 | 1.31 | 0.34 |
| PPEA elastomer | None | 308.8 | 484 | 6.72 ± 0.06 | 2.31 | 2.11 | 0.34 |

*The polymerization degree of effective polymer strands ($N_{eff}$) was determined from the plateau modulus $G'$ using $G' = \rho\phi k_B T/(M_0 N_{eff})$, where $\rho$ is density of dry polymer, $\phi$ is the volume fraction of polymer, $k_B$ is the Boltzmann constant, $T$ is the temperature (K), and $M_0$ is the molecular weight of the monomer. †$\lambda_{max}$ denotes the maximum $\lambda_{tr}$ for cyclic training for training of $N_{tr} = 10^4$ without showing sample fracture.

Furthermore, we conducted cyclic training to a viscoelastic and self-healing poly(ethylene glycol phenyl ether acrylate) (PPEA) elastomer without phase separation and crystallization (figs. S4 and S5) (*55*). The PPEA elastomer exhibited $\lambda_f$(monotonic) = 6.72 and $\lambda_f$(cyclic) = 2.31, resulting in a ratio of $\lambda_f$(cyclic)/$\lambda_f$(monotonic) = 0.34 (Table 1). This further supports the conclusion that the hierarchical structure present in the s-PA gel, which results in multiscale and multistep damage during loading, plays a critical role in sustaining cyclic training over a wide deformation range.

## Training-detraining dynamics

We attempt to make a connection between the dynamic characteristics of s-PA gel during the cyclic training process and its multiscale structures. We used the generalized Maxwell model (Prony series) to analyze plots of $W_{ex}$ and $\lambda_{res}$ versus $N_{tr}$ curve for s-PA gels trained at various $\lambda_{tr}$. It was observed that the first three terms ($n = 3$) of the Prony series were sufficient to fit the $W_{ex}$ versus $N_{tr}$ curves of s-PA gel (fig. S6A). However, only two terms ($n = 2$) of the Prony series were sufficient to fit the $W_{ex}$ versus $N_{tr}$ curves of PPEA elastomer (fig. S6B). Notably, the PPEA exhibited full recovery times for $W_{ex}$ and $\lambda_{res}$ that were one to two orders of magnitude lower than those of s-PA gel trained at the same $\lambda_{tr}$ (table S1). From the two-term Prony series fitting, we obtained two cycle parameters $N_1$(~0.6) and $N_2$(~15) for $W_{ex}$ of the PPEA. Both of them are much smaller than the total training cycle $N_{tr} = 10^4$. These results suggest that the self-healing PPEA elastomer lacks long-term adaptation and memory to cyclic training due to the absence of a hierarchical structure.

Therefore, the first three terms of the Prony series were applied for fitting the results of s-PA gel (see details in section S2 and figs. S7 and S8), from which we obtained three cycle parameters—$N_1$(~1), $N_2$(~20), and $N_3$(~1000)—of three different orders of magnitude. Figure 3A shows the cycle parameters $N_i$ of $W_{ex}$ versus $\lambda_{tr}$. Comparing these $N_1$(~1), $N_2$(~20), and $N_3$(~1000) with the $N_1$(~0.6) and $N_2$(~15) obtained from the PPEA without hierarchical structure, it seems that the $N_3$(~1000) corresponds to the adaptation of phase networks. Specifically, because long-term $N_3$ decreases with $\lambda_{tr}$ at $\lambda_{tr} < \lambda_{affine}$ and becomes almost constant at $\lambda_{affine} < \lambda_{tr} < \lambda_c$ (Fig. 3A), we are able to correlate $N_3$ with the hard-phase network. This is because adaptation is accelerated as a higher oriented hard-phase network forms at a higher $\lambda_{tr}$, whereas further increasing $\lambda_{tr}$ to $\lambda_{affine} < \lambda_{tr} < \lambda_c$ results in damage to the hard-phase network. Because the damaged hard-phase network no longer carries a load, acceleration of the training effect ceases at $\lambda_{affine} < \lambda_{tr} < \lambda_c$. These results indicate that the long-term training memory related to $W_{ex}$ is due to the hard-phase network. However, after the hard-phase network is broken, the soft-phase network with a relatively short relaxation time is not conducive to remembering training effects. By further comparing the fitting parameters with our rheological results, the $N_1$(~1) and $N_2$(~20) seems to be in consistent with short-scale ionic breaking and local adaptation of transient networks, respectively. Consequently, we assign the $N_1$(~1), $N_2$(~20), and $N_3$(~1000) as the characteristic training cycles (with their corresponding times referred to as characteristic training times) for short-scale ionic breaking, local adaptation of transient networks, and adaptation of the hard-phase network, respectively.

The Prony series was also used to fit the evolution of hysteresis energy density $U_{hys}$ (the area between the load and unload curves) of s-PA gel, a parameter related to the energy used to break and rearrange ionic bonds to keep the anisotropic structure. Characteristic training cycles $N_1$, $N_2$, and $N_3$ of $U_{hys}$ are similar to those of $W_{ex}$ (fig. S9). In addition, $N_3$ decreases with $\lambda_{tr}$ for $\lambda_{tr} < \lambda_{affine}$ and remains almost constant for $\lambda_{affine} < \lambda_{tr} < \lambda_c$. These results imply that long-term adaptation of energy dissipation in the training process depends on whether damage occurs in the hard-phase network.

The evolution of $W_{ex}$ and $U_{hys}$ reflects the energy dissipation contributed by the hierarchical structures, whereas $\lambda_{res}$ is related to the conformation of the hierarchical structures. As demonstrated in our previous work, the recovery of $\lambda_{res}$ is dominated by the soft-phase network, which remains intact in training process. Therefore, characteristic training cycles $N_1$, $N_2$, and $N_3$ of $\lambda_{res}$ show little dependence on $\lambda_{tr}$ (Fig. 3B).

The three-term Prony series was also used to fit the $W_{ex}(t_{rest})$ and $\lambda_{res}(t_{rest})$ versus $t_{rest}$ curves during the detraining processes of s-PA gel (see details in section S3 and figs. S10 and S11). It shows that the irrecoverable term $w_\infty$ increases with $\lambda_{tr}$ at $\lambda_{affine} < \lambda_{tr} < \lambda_c$ (fig. S10D), indicating increased damage to the hard-phase network. Figure S10E shows that characteristic detraining times $\tau_{f,1}$, $\tau_{f,2}$, and $\tau_{f,3}$ of $W_{ex}(t_{rest})$ increase with $\lambda_{tr}$ (data also in Fig. 3C). However, the slopes of $\tau_{f,i}$ versus $\lambda_{tr}$ at $\lambda_{tr} < \lambda_{affine}$ were larger than those at $\lambda_{affine} < \lambda_{tr} < \lambda_c$. This indicates that maintaining an intact hard-phase network during the training process benefits memory of the training effect. However, once the hard-phase network suffers damage, the soft-phase network (with relatively fast dynamics) weakens memory. Figure S11D shows that the characteristic detraining times $\tau_{f,1}$, $\tau_{f,2}$, and $\tau_{f,3}$ of $\lambda_{res}(t_{rest})$ increase with $\lambda_{tr}$ at $\lambda_{tr} < \lambda_{affine}$ but show a weak dependence on $\lambda_{tr}$ at $\lambda_{affine} < \lambda_{tr} < \lambda_c$ (data also shown in Fig. 3D). The former is correlated with the memory of the intact hard-phase network, whereas the latter can be

attributed to the relatively fast dynamics of the soft-phase network after damage to the hard-phase network.

In addition to training intensity $\lambda_{tr}$, we investigated the effect of training duration $N_{tr}$ on detraining dynamics. As shown in fig. S12, detraining is slower for larger $N_{tr}$. Characteristic detraining times $\tau_{f,1}$, $\tau_{f,2}$, and $\tau_{f,3}$ of $W_{ex}(t_{rest})$ and $\lambda_{res}(t_{rest})$ increase sharply during the first 1000 cycles and then reach a plateau (fig. S12, E and F), indicating that training saturation occurs for $N_{tr} > 1000$. Therefore, all training experiments performed above were conducted at saturation training conditions.

A comparison between the characteristic training and detraining times of the s-PA gel subjected to saturation training (Fig. 3, C and D) suggests that $W_{ex}$ has asymmetric dynamics, whereas $\lambda_{res}$ is more like symmetric dynamics. Characteristic detraining times $\tau_{f,i}$ of $W_{ex}$ are approximately one order of magnitude larger than characteristic training times $\tau_i$ of the same terms (Fig. 3C). The difference between $\tau_{f,i}$ and $\tau_i$ of $W_{ex}$ becomes more notable when $\lambda_{affine} < \lambda_{tr} < \lambda_c$. However, $\tau_{f,2}$ and $\tau_{f,3}$ of $\lambda_{res}$ have almost the same values as $\tau_2$ and $\tau_3$ regardless of $\lambda_{tr} < \lambda_{affine}$ or $\lambda_{affine} < \lambda_{tr} < \lambda_c$, and $\tau_1$ is slightly larger than $\tau_{f,1}$ at $\lambda_{affine} < \lambda_{tr} < \lambda_c$ (Fig. 3D). The asymmetric dynamics of $W_{ex}$ can be attributed to the slow dynamics of hard-phase network. When training is performed at $\lambda_{tr} < \lambda_{affine}$, the rearranged ionic bonds in the intact hard-phase network reform the original pairs very slowly because of restricted mobility. When training is performed at $\lambda_{affine} < \lambda_{tr} < \lambda_c$, the ionic bonds in the damaged hard-phase network could not find the original pairs, resulting in an increase in the irrecoverable $w_\infty$ (fig. S10D). Therefore, $\tau_{f,i}$ of $W_{ex}$ are always larger than that of $\tau_i$. The symmetric dynamics of $\lambda_{res}$ can be attributed to the relatively fast dynamics of soft-phase network. In a similar manner to DN gels (*56*–*58*), when the hard-phase network is damaged, the soft-phase network can retract the sample back to its original size. Thus, $\lambda_{res}$ can recover to 1.0 during detraining (Fig. 2E), which agrees with our previous findings of single-cycle loading of PA gels (*51*).

## Effects of training, overtraining, and detraining on fatigue resistance

Our results show that the memory of training-effect is gradually enhanced with training intensity $\lambda_{tr}$ until $\lambda_{tr} \approx \lambda_{affine}$, (i.e., the onset of damage to the hard-phase network). The question is how training affects the fatigue resistance of the PA gel and whether overtraining occurs at $\lambda_{tr} > \lambda_{affine}$. To answer the questions, we performed fatigue tests on the trained samples to investigate their crack resistance by playing with the $\lambda_{tr}$, $N_{tr}$, and $t_{rest}$. Unnotched samples were first cyclic trained at $\lambda_{tr}$ for $N_{tr}$ cycles and then rested in a strain-free state for $t_{rest}$. Last, we cut a crack at the edge of the samples. Then, we performed fatigue tests at $\lambda_{fatigue} = 2.9$ to track the crack growth length $c$ with the fatigue test cycle $N_{fatigue}$ (Fig. 4A). We chose $\lambda_{fatigue} = 2.9$ because, under this condition, the fatigue crack propagation in the steady state is in slow mode when a notched pristine sample is used for direct fatigue test (*49*, *50*).

First, we demonstrated the effect of training intensity $\lambda_{tr}$ on fatigue resistance. Unnotched samples were trained at $\lambda_{tr} = 2.9 < \lambda_{affine}$ and $\lambda_{tr} = 3.7 > \lambda_{affine}$ for $N_{tr} = 2000$. Loading-unloading curves during training are shown in fig. S13. Note that saturation training occurred at $N_{tr} = 2000$ (fig. S12). To avoid self-recovery, we cut the crack and immediately ($t_{rest} \approx 0$) performed the fatigue test at $\lambda_{fatigue} = 2.9$ after the samples finished their cyclic training. Results are shown in Fig. 4 (B and C). The sample trained at $\lambda_{tr} = 3.7 > \lambda_{affine}$ shows that the crack advances rapidly with $N_{fatigue}$ until the entire sample fractures (Fig. 4C), indicating the occurrence of overtraining. The overtraining weakens crack resistance compared with the untrained pristine sample, resulting in a relatively sharp crack tip (Fig. 4B) (the radius of curvature at the crack tip (fig. S14 and Table 2) is $R = 0.77$ cm at $\lambda_{fatigue} = 2.9$ and $N_{fatigue} = 1800$]. By contrast, the sample trained at $\lambda_{tr} = 2.9 < \lambda_{affine}$ shows that the crack grows at the beginning, and then it is suppressed and hardly advances at a length of $c = 2.7$ mm after $N_{fatigue} \approx 1000$ (Fig. 4C). In this case, crack blunting is observed (Fig. 4B) [the radius of curvature at

**Table 2. Fatigue-resistance of the s-PA gel with different training and detraining history.**

| Sample training history | $t_{rest}$ | Fatigue fracture* | Radius of curvature at crack tip $R$ (cm) | Energy release rate $G_{load}$ (J/m$^2$) | Energy release rate $G_{unload}$ (J/m$^2$) | Crack growth rate (μm/cycle) |
|---|---|---|---|---|---|---|
| Pristine | – | No | 1.83 ($N_{fatigue} = 9 \times 10^3$) | 291.7† | 171.8† | 0.021 |
| $\lambda_{tr} = 2.9$, $N_{tr} = 2 \times 10^3$ | 0 s | No | 1.80 ($N_{fatigue} = 9 \times 10^3$) | 281.4† | 159.2† | 0.027 |
| $\lambda_{tr} = 3.7$, $N_{tr} = 2 \times 10^3$ | 0 s | Fracture | 0.77 ($N_{fatigue} = 1.8 \times 10^3$) | 276.9† | 152.9† | 19.1 |
| $\lambda_{tr} = 3.7$, $N_{tr} = 200$ | 0 s | No | 1.56 ($N_{fatigue} = 9 \times 10^3$) | 310.1† | 158.3† | 0.027 |
| $\lambda_{tr} = 3.7$, $N_{tr} = 2 \times 10^3$ | 55 hours | No | 1.73 ($N_{fatigue} = 9 \times 10^3$) | 274.8† | 158.7† | 0.015 |
| $\lambda_{tr} = 7.1$, $N_{tr} = 10^4$ | 10 days | Fracture | 0.59 ($N_{fatigue} = 500$) | 308.2‡ | 150.5‡ | 53.3 |

*The fatigue test is performed at $\lambda_{fatigue} = 2.9$. No fatigue fracture denotes the crack did not grow more than 25 mm in length within $N_{fatigue} = 4 \times 10^4$ cycles. †Obtained at $N_{fatigue} = 2 \times 10^3$ cycles. ‡Obtained at $N_{fatigue} = 980$ cycles. To obtain the energy release rate, the stress of all the samples was correlated with the effective cross-sectional area of the sample at the corresponding $N_{fatigue}$.

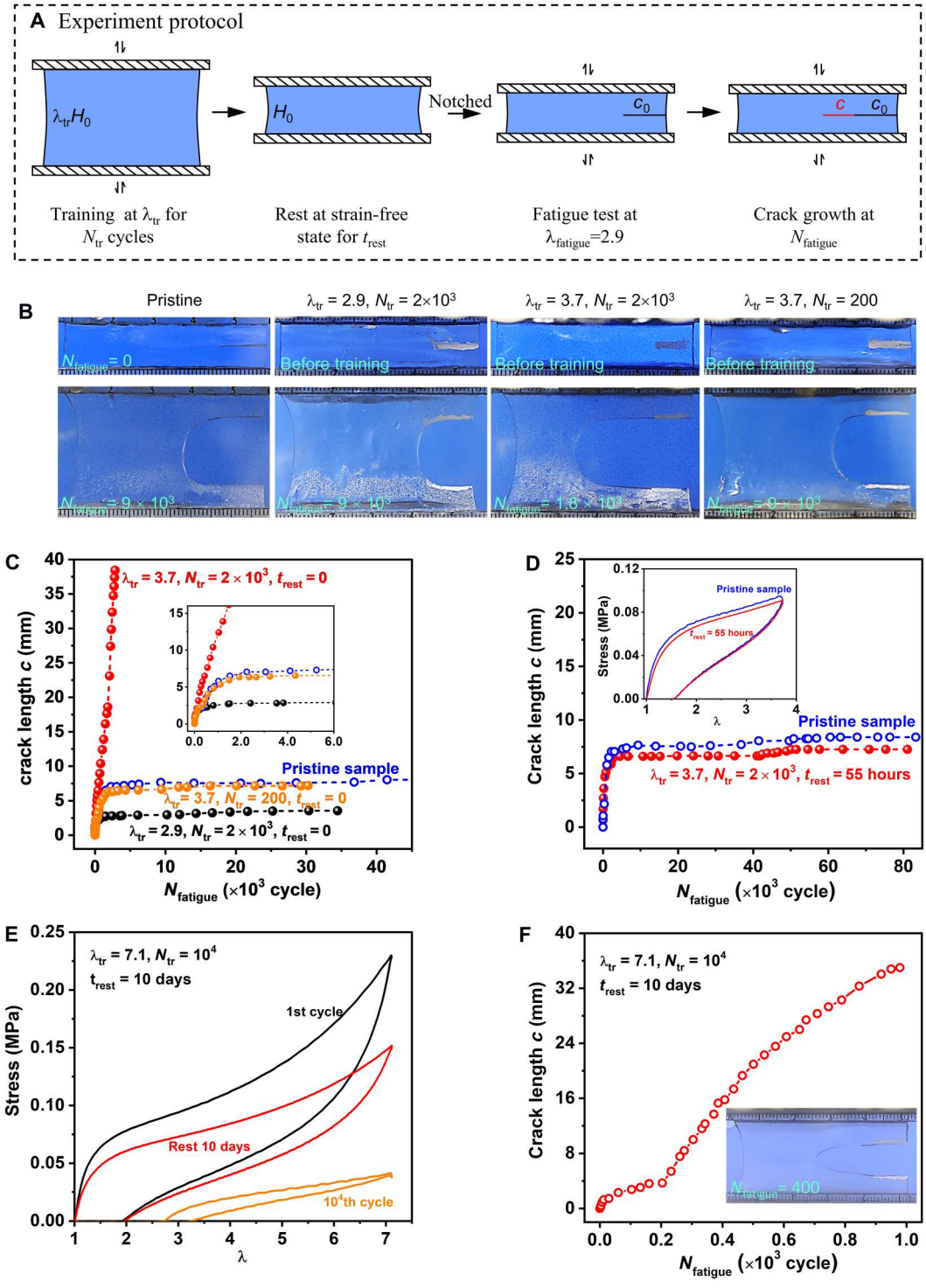


**Fig. 4. Role of training intensity ($\lambda_{tr}$), training duration ($N_{tr}$), and rest time ($t_{rest}$) on fatigue resistance of s-PA gel.** (**A**) Experimental protocol. The unnotched sample was trained at stretching ratio $\lambda_{tr}$ for $N_{tr}$ cycles, then allowed to rest for time $t_{rest}$, after which the sample was notched ($c_0$ = 10 mm), and then immediately subjected to fatigue testing at $\lambda_{fatigue}$ = 2.9 for $N_{fatigue}$ cycles to observe crack resistance. Crack growth length is denoted as $c$. (**B** and **C**) Typical crack tip shape (B) and fatigue crack propagation behavior (C) for samples trained at $\lambda_{tr}$ = 2.9 for $N_{tr}$ = 2000 and $\lambda_{tr}$ = 3.7 for $N_{tr}$ = 2000 and 200 with $t_{rest}$ = 0. Inset is a zoom-in view of the initial 6000 cycles. (**D**) Fatigue results for the sample experienced mild overtraining ($\lambda_{tr}$ = 3.7 for $N_{tr}$ = 2000) and resting for $t_{rest}$ = 55 hours. Inset shows the loading-unloading curve of the rested sample compared to the pristine sample. (**E** and **F**) Loading-unloading curves for gel trained at $\lambda_{tr}$ = 7.1 for $N_{tr}$ = $10^4$ and allowed to rest for $t_{rest}$ = 10 days (E), and its fatigue test result (F).

the crack tip (fig. S14 and Table 2) is $R$ = 1.80 cm at $\lambda_{fatigue}$ = 2.9 and $N_{fatigue}$ = 9000], and crack resistance is higher than the untrained pristine sample (i.e., the crack stops at $c$ = 7 mm after $N_{fatigue} \approx$ 2000). That suggests that the crack resistance of the sample trained at $\lambda_{tr} = 2.9 < \lambda_{affine}$ for $N_{tr}$ = 2000 is reinforced by the rearrangement of the transient and phase networks, effectively reducing adaptation time in the fatigue test.

Training-reinforcing crack resistance at $\lambda_{tr} < \lambda_{affine}$ and overtraining at $\lambda_{tr} > \lambda_{affine}$ results presented here have some connection with the direct fatigue test using pre-notched PA gels in our previous studies (*49*, *50*). We observed a slow-to-fast transition in steady-state crack propagation for $\lambda_{fatigue} = \lambda_{tran}$ with the crack propagation rate increasing by several orders of magnitude (where $\lambda_{tran}$ is the slow-to-fast mode transition stretch ratio in the direct fatigue test). The hydrogel with the same formulation as in this study shows $\lambda_{tran}$ = 3.1, which is close to $\lambda_{affine}$. For $\lambda_{fatigue} < \lambda_{affine}$, bicontinuous phase networks in the bulk specimen remained intact and self-trained into an oriented structure, suppressing crack propagation (*50*). Circular polarization results show that the fatigue test before the steady state at $\lambda_{fatigue} < \lambda_{affine}$ leads to self-training both in the bulk specimen and at the crack tip, weakening the stress concentration around the crack tip (section S4 and fig. S15B). Stress concentration always occurs when $\lambda_{fatigue} > \lambda_{affine}$, resulting in overtraining and cracks accelerating to the fast mode (section S4 and fig. S15C) (*50*).

Fatigue resistance deterioration is an intuitive result of overtraining. Therefore, attention should be paid to avoid overtraining. We investigated how overtraining can be avoided in a PA gel for a large $\lambda_{tr}$ and found that unnotched gels trained at $\lambda_{tr}$ = 3.7 for fewer cycles (e.g., $N_{tr}$ = 200 cycles) exhibited the same fatigue resistance as a pristine sample. The radius of curvature at the crack tip is $R$ = 1.56 cm at $\lambda_{fatigue}$ = 2.9 and $N_{fatigue}$ = 9000, close to that of the untrained pristine sample (fig. S14 and Table 2). This result starkly contrasted with samples trained at $\lambda_{tr}$ = 3.7 for $N_{tr}$ = 2000 cycles (Fig. 4, B and C). The difference can be attributed to less accumulated damage for $N_{tr}$ = 200 cycles than for $N_{tr}$ = 2000 cycles (fig. S12). In addition, even when gels suffer from mild overtraining ($\lambda_{tr}$ = 3.7, $N_{tr}$ = 2000), their loading-unloading curves and fatigue resistance almost completely recover after a 55-hour rest period (Fig. 4D). That suggests that the damaged hard-phase network heals after a sufficiently long rest, implying that this overtraining does not cause severe internal fractures. The above results suggest two effective ways of avoiding overtraining despite relatively large deformations: (i) minimize the number of training cycles to reduce damage accumulation and (ii) rest and await healing (*59*–*61*).

It should be noted that fatal overtraining occurs when $\lambda_{tr}$ is much greater than $\lambda_{affine}$, as shown in Fig. 4 (E and F), which depict examples of fatal overtraining at $\lambda_{tr}$ = 7.1 for $N_{tr} = 10^4$. Although the residual stretch ratio $\lambda_{res}$ recovered completely, the softening of the stress remains even after resting for 10 days. That suggests that permanent damage occurred in the hard-phase network (probably a large amount of polymer chains chemically rupture in the hard-phase network, because $\lambda_{tr}$ far exceeds the strain-hardening limit). It results in fatal overtraining, markedly weakening fatigue resistance to crack growth even after prolonged rest, as shown in Fig. 4F. Table 2 shows that the fatally overtrained sample have a small radius of curvature at the crack tip ($R$ = 0.59 cm at $\lambda_{fatigue}$ = 2.9 and $N_{fatigue}$ = 500). This is in sharp contrast to the pre-notched pristine sample, which exhibits crack blunting and consequently results in an extremely slow crack growth rate (Table 2). However, the soft-phase network (due to its relatively fast dynamics) enabled the gel to revert to its original shape (*51*), resulting in no residual stretch ratio after resting.

The energy release rate $G$, defined as the energy used for fatigue crack growth, is obtained by $G_{load} = W_{ex} \times H_0$ and $G_{unload} = W_{el} \times H_0$. Here, $H_0$ = 10 mm is the undeformed sample height. $W_{ex}$ and $W_{el}$ refer to the area under the loading and unloading curves of the s-PA gel at the steady state of fatigue test. The stress of the samples with different training and resting histories was correlated with the effective cross-sectional area of the sample at the corresponding $N_{fatigue}$. Typically, $N_{fatigue} \approx$ 2000 denoted the steady state for samples exhibiting crack blunting. However, in the case of the sample that underwent overtraining at $\lambda_{tr}$ = 7.1 for $N_{tr} = 10^4$ and resting for 10 days, it fractured before reaching 2000 cycles. In this case, we utilized the stress-stretch curve at $N_{fatigue}$ = 980 to determine the $G$.

It is quite unexpected to discover that samples with varying training and resting histories exhibit similar $G_{load}$ or $G_{unload}$ values, despite the crack growth rates differing by three orders of magnitude (Table 2). This phenomenon may be attributed to three reasons. First it is probably due to the fast mechanical adaptation characteristic of the PA gel, stemming from the entropy elasticity of the polymer network and the quick self-healing properties of ionic bonds (fig. S16). Second, the unbroken or self-healing ionic bonds may contribute more to the energy release rate than the polymer network at the high strain rate of 1 $s^{-1}$. In our previous work (*47*), we predicted the fatigue threshold $G_0^{th}$ = 10 J/$m^2$ for s-PA gel using the Lake-Thomas model (*62*), and we obtained a fatigue threshold of $G_0^{elastic}$ = 27.3 J/$m^2$ for s-PA gel when we extended our observation timescale to the relatively elastic regime (strain rate of $10^{-4}$ $s^{-1}$) by using the time-salt superposition principle. Both of these values are lower than the experimental fatigue threshold of $G_0^{exp}$ = 70 J/$m^2$ for s-PA gel under fatigue test at a strain rate of 1 $s^{-1}$, even the $G_0^{exp}$ was calculated from the unloading curve in the steady state (*49*). This suggests that, for fatigue tests at a strain rate of 1 $s^{-1}$, the ionic bonds play a substantial role in contributing to the energy release rate $G$. Third, the local energy for crack propagation may differ from the applied energy release rate $G$. Because of the viscoelastic dissipation in bulk material, the applied $G$ is difficult to transfer to the crack tip, which may overestimate the actual $G$ by using the applied $G$ for the crack unextended area (*63*).

## DISCUSSION

We demonstrated that a tough self-healing hydrogel composed of hierarchical structures exhibits mechanically effective training, overtraining, and detraining behaviors. Cyclic training was performed under two conditions: (i) at $\lambda_{tr} < \lambda_{affine}$, where both the hard- and soft-phase networks are intact; and (ii) at $\lambda_{affine} < \lambda_{tr} < \lambda_c$, where damage in the hard-phase network occurs, while the soft-phase network stays intact. Notably, we discovered that the soft material lacking a hierarchical structure demonstrates substantially lower extensibility under cyclic stretching compared to monotonic stretching. In contrast, s-PA gel, which has a hierarchical structure, can sustain considerably high deformation during cyclic stretching, approaching the fracture limit observed during monotonic stretching. In addition, the s-PA gel exhibits a long-term

adaptation and memory to the cyclic training effect. By combining viscoelastic model fitting and fatigue tests, we demonstrated that long-term adaptation of energy dissipation (compliance) depends on the hard-phase network with a restricted mobility and slow dynamics. Whereas shape-adaptation of hierarchical structures depends on the soft-phase network with fast dynamics. Compliance changes during training/detraining exhibit asymmetric dynamics, whereas gel shape changes are more symmetric.

Training under condition i reinforces crack resistance for a subsequent fatigue test due to the accumulated rearrangement of transient and phase networks. However, overtraining occurs under condition ii, which markedly decreases fatigue resistance due to accumulated damage in the hard-phase network. For mild overtraining around $\lambda_{affine}$, the damaged structure can self-heal after a sufficiently long rest time. Fatal overtraining at $\lambda_{tr} >> \lambda_{affine}$ causes permanently weakened performance. Although temperature variations undoubtedly affect training-detraining dynamics, our study was performed under constant-temperature conditions. Cyclic training adaptation mechanisms in tough self-healing hydrogels revealed in this study provide insights into developing soft materials with long-term mechanical adaptation.

## MATERIALS AND METHODS

### Materials

The anionic monomer NaSS, cationic monomer DMAEA-Q, chemical cross-linker *N*,*N*′-methylenebis(acrylamide) (MBAA), and ultraviolet (UV) initiator α-ketoglutaric acid (α-keto) were purchased from Wako Pure Chemical Industries Ltd. and used as received. Ethylene glycol phenyl ether acrylate (PEA) was supplied by Osaka Organic Chemical Industry Ltd., Japan, and used as received. A UV initiator, benzophenone (BP; KANTO Chemical Co. Inc.), was used to initiate PEA polymerization. Deionized water was used in all experiments.

### Synthesis of PA hydrogels

We synthesized the PA hydrogel using one-step random copolymerization of NaSS and DMAEA-Q, around the point of charge balance in the presence of MBAA and α-keto, following procedures in (*44*, *64*, *65*). First, a mixed aqueous solution of total monomers $C_m$ = 2.0 M with an optimized molar fraction of NaSS $f$ = 0.515, 0.1 mol % MBAA, and 0.1 mol % α-keto (both relative to total monomer concentration $C_m$) was prepared. Then, the solution was injected into a (20 cm by 20 cm) reaction cell consisting of a pair of glass plates with a 2-mm silicone spacer in an argon atmosphere. That was followed by UV irradiation to initiate polymerization (11 hours). Last, the as-prepared gel was dialyzed in 30°C deionized water for 3 weeks to remove counterions and reach a water-equilibrated state. Deionized water was exchanged daily. During dialysis, the gel de-swelled owing to attractive electrostatic interactions between positive and negative charges on the polymer chains. Mesoscale bicontinuous hard/soft-phase networks were formed during the dialysis process (*66*). This water-equilibrated hydrogel exhibiting strong-phase separation (high modulus contrast between the hard- and soft-phase domains) is denoted as s-PA gel.

The PA gel with weak-phase separation (w-PA) was prepared by the same procedures as that of s-PA except that the total monomer concentration was $C_m$ = 2.5 M and the chemical cross-linker content was 0.5 mol %. The w-PA gel exhibits very weak-phase separation (fig. S3A).

### Synthesis of PPEA elastomer

PPEA elastomer was synthesized following procedures in (*55*). In short, after the 0.1 mol % UV initiator BP and 0.1 mol % chemical cross-linker MBAA were dissolved into monomer PEA, we injected the solution into a (10 cm by 20 cm) reaction cell consisting of a pair of glass plates with a 1.5-mm silicone spacer in an argon atmosphere. Then, the reaction cell was irradiated by UV to initiate polymerization. The total polymerization time was 11 hours. The obtained PPEA elastomer was stored at 24°C for use. The PPEA elastomer does not exhibit phase separation (fig. S4C) or crystallization but has good self-healing property (*55*).

### Cyclic training and detraining

Cyclic training was performed using a Shimadzu tensile tester (100-N load cell, AG-X, Shimadzu Corporation). Unnotched samples with pure shear geometry were used (Fig. 2A). A humidity chamber was set on the tensile tester to sustainably supply water vapor to prevent dehydration of the PA gels. Cyclic loading-unloading was performed along the sample height $H_0$ direction at a nominal strain rate of 1 $s^{-1}$. Room temperature was maintained at 24°C. Loading-unloading curves were recorded. Stress was defined as the force over the initial undeformed cross-sectional area, and stretch ratio λ was defined as the ratio between the deformed and initial sample height. A triangular loading profile was used for cyclic training: The maximum stretch ratio in each cycle was preset at $\lambda_{tr}$ and the minimum at $\lambda_{min}$ = 1 (fig. S7A). To test the recovery efficiency during detraining (or rest), we performed one loading cycle using the same conditions as cyclic training after the sample rested for preset times ($t_{rest}$). In all experiments, the samples did not dry or part dry, as confirmed by no weight change before and after training, detraining, or fatigue tests. The monotonic stretching of PA gels with the pure shear geometry was also performed at 24°C under a strain rate of 1 $s^{-1}$.

Cyclic training of PPEA elastomer was conducted with the same training-detraining procedures as that of PA gels except that the strain rate was 0.5 $s^{-1}$, and no water vapor was required to supply. The monotonic stretching of PPEA elastomer with the pure shear geometry was also performed at 24°C under a strain rate of 0.5 $s^{-1}$.

### Fatigue test

Direct fatigue tests of pristine samples were performed using notched samples with a pure shear geometry (initial crack length $c_0$ = 10 mm; fig. S15A). A triangular loading profile was used for fatigue tests. Consecutive cyclic loading without rest was performed at $\lambda_{fatigue}$ = 2.7 and 3.5, and the minimum was maintained at $\lambda_{min}$ = 1. The nominal strain rate was 1 $s^{-1}$, and the temperature was 24°C. A homemade circular polarizing optical system was used to measure the birefringence in the fatigue test following the method described in (*50*, *67*).

The fatigue test of the trained sample was performed as follows. After the unnotched gel suffered from training at $\lambda_{tr}$ for $N_{tr}$ and rested for $t_{rest}$, we made a notch ($c_0$ = 10 mm) at the edge of the sample and then performed fatigue tests at a preset stretch ratio $\lambda_{fatigue}$ of 2.9 under a strain rate of 1 $s^{-1}$ (Fig. 4A).

### Time-resolved SAXS measurements

To detect the deformation of bicontinuous phase networks during cyclic training, in situ time-resolved SAXS measurements were carried out at the Synchrotron Radiation Facility (BL19U2, Shanghai, China) using unnotched rectangular samples (7.5 mm by 16 mm by 1.65 mm, $L_0 \times H_0 \times t_0$) (fig. S1). A 2D detector (Pilatus 1 M with a resolution of 981 × 1043 pixels and a pixel size of 172 μm, Dectris Co. Ltd.) was used to record the data. The x-ray wavelength and sample-to-detector distance were 1.03 Å and 5730 mm, respectively. A tensile machine with well-controlled humidity and temperature was used for the cyclic training. The nominal strain rate was 1 $s^{-1}$, and the temperature was 24°C. 2D SAXS patterns were acquired at a rate of 0.25 s per frame. SAXS data were analyzed using Fit 2D software from the European Synchrotron Radiation Facility, and background scattering from the air was subtracted. The 2D SAXS patterns were integrated along the azimuthal direction to obtain 1D scattering profiles as a function of scattering vector $q = 4\pi\sin\theta/\lambda$, where $q$ is the module of the scattering vector, λ is the x-ray wavelength, and 2θ is the scattering angle. From the peak position of 1D scattering profiles ($q_{max}$), we obtained the $d$-spacing of the phase structure ($d = 2\pi/q_{max}$).

## Supplementary Materials

**This PDF file includes:**

Figs. S1 to S16
Sections S1 to S4
Table S1
References

## REFERENCES AND NOTES


1. M. P. McHugh, C. H. Cosgrave, To stretch or not to stretch: The role of stretching in injury prevention and performance. *Scand. J. Med. Sci. Sports* **20**, 169–181 (2010).
2. I. Mujika, S. Padilla, Detraining: Loss of training-induced physiological and performance adaptations. Part II: Long term insufficient training stimulus. *Sports Med.* **30**, 145–154 (2000).
3. I. Mujika, S. Padilla, Detraining: Loss of training-induced physiological and performance adaptations. Part I: Short term insufficient training stimulus. *Sports Med.* **30**, 79–87 (2000).
4. N. Matos, R. J. Winsley, Trainability of young athletes and overtraining. *J. Sports Sci. Med.* **6**, 353–367 (2007).
5. L. L. Smith, Tissue trauma: The underlying cause of overtraining syndrome? *J. Strength Cond. Res.* **18**, 185–193 (2004).
6. T. Nonoyama, J. P. Gong, Tough double network hydrogel and its biomedical applications. *Annu. Rev. Chem. Biomol. Eng.* **12**, 393–410 (2021).
7. T. Matsuda, R. Kawakami, R. Namba, T. Nakajima, J. P. Gong, Mechanoresponsive self-growing hydrogels inspired by muscle training. *Science* **363**, 504–508 (2019).
8. Z. J. Wang, J. Jiang, Q. Mu, S. Maeda, T. Nakajima, J. P. Gong, Azo-crosslinked double-network hydrogels enabling highly efficient mechanoradical generation. *J. Am. Chem. Soc.* **144**, 3154–3161 (2022).
9. S. Lin, J. Liu, X. Liu, X. Zhao, Muscle-like fatigue-resistant hydrogels by mechanical training. *Proc. Natl. Acad. Sci. U.S.A.* **116**, 10244–10249 (2019).
10. J. N. Jin, X. R. Yang, Y. F. Wang, L. M. Zhao, L. P. Yang, L. Huang, W. Jiang, Mechanical training enabled reinforcement of polyrotaxane-containing hydrogel. *Angew. Chem. Int. Ed. Engl.* **62**, e202218313 (2023).
11. Z. Lei, W. Gao, W. Zhu, P. Wu, Anti-fatigue and highly conductive thermocells for continuous electricity generation. *Adv. Funct. Mater.* **32**, 2201021 (2022).
12. Z. Wang, J. Tang, R. Bai, W. Zhang, T. Lian, T. Lu, T. Wang, A phenomenological model for shakedown of tough hydrogels under cyclic loads. *J. Appl. Mech.* **85**, 091005 (2018).
13. Y. Zhou, J. Hu, P. Zhao, W. Zhang, Z. Suo, T. Lu, Flaw-sensitivity of a tough hydrogel under monotonic and cyclic loads. *J. Mech. Phys. Solids* **153**, 104483 (2021).
14. R. Bai, J. Yang, Z. Suo, Fatigue of hydrogels. *Eur. J. Mech. A Solids* **74**, 337–370 (2019).
15. J. Tang, J. Li, J. J. Vlassak, Z. Suo, Fatigue fracture of hydrogels. *Extreme Mech. Lett.* **10**, 24–31 (2017).
16. W. Zhang, J. Hu, H. Yang, Z. Suo, T. Lu, Fatigue-resistant adhesion II: Swell tolerance. *Extreme Mech. Lett.* **43**, 101182 (2021).
17. C. Xiang, Z. Wang, C. Yang, X. Yao, Y. Wang, Z. Suo, Stretchable and fatigue-resistant materials. *Mater. Today* **34**, 7–16 (2020).
18. E. Zhang, R. Bai, X. P. Morelle, Z. Suo, Fatigue fracture of nearly elastic hydrogels. *Soft Matter* **14**, 3563–3571 (2018).
19. J. Ni, S. Lin, Z. Qin, D. Veysset, X. Liu, Y. Sun, A. J. Hsieh, R. Radovitzky, K. A. Nelson, X. Zhao, Strong fatigue-resistant nanofibrous hydrogels inspired by lobster underbelly. *Matter* **4**, 1919–1934 (2021).
20. X. Liang, G. Chen, S. Lin, J. Zhang, L. Wang, P. Zhang, Y. Lan, J. Liu, Bioinspired 2D isotropically fatigue-resistant hydrogels. *Adv. Mater.* **34**, e2107106 (2022).
21. M. Hua, S. Wu, Y. Ma, Y. Zhao, Z. Chen, I. Frenkel, J. Strzalka, H. Zhou, X. Zhu, X. He, Strong tough hydrogels via the synergy of freeze-casting and salting out. *Nature* **590**, 594–599 (2021).
22. S. Lin, X. Liu, J. Liu, H. Yuk, H.-C. Loh, G. A. Parada, C. Settens, J. Song, A. Masic, G. H. McKinley, Anti-fatigue-fracture hydrogels. *Sci. Adv.* **5**, eaau8528 (2019).
23. G. Zhang, J. Kim, S. Hassan, Z. Suo, Self-assembled nanocomposites of high water content and load-bearing capacity. *Proc. Natl. Acad. Sci. U.S.A.* **119**, e2203962119 (2022).
24. J.-Y. Sun, X. Zhao, W. R. Illeperuma, O. Chaudhuri, K. H. Oh, D. J. Mooney, J. J. Vlassak, Z. Suo, Highly stretchable and tough hydrogels. *Nature* **489**, 133–136 (2012).
25. J. Li, Z. Suo, J. J. Vlassak, Stiff, strong, and tough hydrogels with good chemical stability. *J. Mater. Chem. B* **2**, 6708–6713 (2014).
26. R. Bai, J. Yang, X. P. Morelle, C. Yang, Z. Suo, Fatigue fracture of self-recovery hydrogels. *ACS Macro Lett.* **7**, 312–317 (2018).
27. P. Lin, S. Ma, X. Wang, F. Zhou, Molecularly engineered dual-crosslinked hydrogel with ultrahigh mechanical strength, toughness, and good self-recovery. *Adv. Mater.* **27**, 2054–2059 (2015).
28. H. C. Yu, S. Y. Zheng, L. Fang, Z. Ying, M. Du, J. Wang, K. F. Ren, Z. L. Wu, Q. Zheng, Reversibly transforming a highly swollen polyelectrolyte hydrogel to an extremely tough one and its application as a tubular grasper. *Adv. Mater.* **32**, e2005171 (2020).
29. H. Sun, S. Li, K. Li, Y. Liu, C. Tang, Z. Liu, L. Zhu, J. Yang, G. Qin, Q. Chen, Tough and self-healable carrageenan-based double network microgels enhanced physical hydrogels for strain sensor. *J. Polym. Sci.* **60**, 2720–2732 (2021).
30. Q. Chen, L. Zhu, C. Zhao, Q. Wang, J. Zheng, A robust, one-pot synthesis of highly mechanical and recoverable double network hydrogels using thermoreversible sol-gel polysaccharide. *Adv. Mater.* **25**, 4171–4176 (2013).
31. R. Long, K. Mayumi, C. Creton, T. Narita, C.-Y. Hui, Time dependent behavior of a dual cross-link self-healing gel: Theory and experiments. *Macromolecules* **47**, 7243–7250 (2014).
32. K. Mayumi, J. Guo, T. Narita, C. Y. Hui, C. Creton, Fracture of dual crosslink gels with permanent and transient crosslinks. *Extreme Mech. Lett.* **6**, 52–59 (2016).
33. K. Mayumi, A. Marcellan, G. Ducouret, C. Creton, T. Narita, Stress–strain relationship of highly stretchable dual cross-link gels: Separability of strain and time effect. *ACS Macro Lett.* **2**, 1065–1068 (2013).
34. M. Rodin, J. Li, D. Kuckling, Dually cross-linked single networks: Structures and applications. *Chem. Soc. Rev.* **50**, 8147–8177 (2021).
35. T. Narita, K. Mayumi, G. Ducouret, P. Hébraud, Viscoelastic properties of poly(vinyl alcohol) hydrogels having permanent and transient cross-links studied by microrheology, classical rheometry, and dynamic light scattering. *Macromolecules* **46**, 4174–4183 (2013).
36. V. Yesilyurt, M. J. Webber, E. A. Appel, C. Godwin, R. Langer, D. G. Anderson, Injectable self-healing glucose-responsive hydrogels with pH-regulated mechanical properties. *Adv. Mater.* **28**, 86–91 (2016).
37. M. Ohira, T. Katashima, M. Naito, D. Aoki, Y. Yoshikawa, H. Iwase, S. I. Takata, K. Miyata, U. I. Chung, T. Sakai, M. Shibayama, X. Li, Star-polymer-DNA gels showing highly predictable and tunable mechanical responses. *Adv. Mater.* **34**, e2108818 (2022).
38. V. Yesilyurt, A. M. Ayoob, E. A. Appel, J. T. Borenstein, R. Langer, D. G. Anderson, Mixed reversible covalent crosslink kinetics enable precise, hierarchical mechanical tuning of hydrogel networks. *Adv. Mater.* **29**, 1605947 (2017).
39. M. Zhang, D. Xu, X. Yan, J. Chen, S. Dong, B. Zheng, F. Huang, Self-healing supramolecular gels formed by crown ether based host-guest interactions. *Angew. Chem. Int. Ed. Engl.* **51**, 7011–7015 (2012).
40. A. Harada, Y. Takashima, A. Hashidzume, H. Yamaguchi, Supramolecular polymers and materials formed by host-guest interactions. *Bull. Chem. Soc. Jpn.* **94**, 2381–2389 (2021).
41. M. Nakahata, Y. Takashima, A. Harada, Highly flexible, tough, and self-healing supramolecular polymeric materials using host-guest interaction. *Macromol. Rapid Commun.* **37**, 86–92 (2016).
42. R. S. Staron, M. J. Leonardi, D. L. Karapondo, E. S. Malicky, J. E. Falkel, F. C. Hagerman, R. S. Hikida, Strength and skeletal muscle adaptations in heavy-resistance-trained women after detraining and retraining. *J. Appl. Physiol.* **70**, 631–640 (1991).

43. K. M. Wisdom, S. L. Delp, E. Kuhl, Use it or lose it: Multiscale skeletal muscle adaptation to mechanical stimuli. *Biomech. Model. Mechanobiol.* **14**, 195–215 (2015).
44. T. L. Sun, T. Kurokawa, S. Kuroda, A. B. Ihsan, T. Akasaki, K. Sato, M. A. Haque, T. Nakajima, J. P. Gong, Physical hydrogels composed of polyampholytes demonstrate high toughness and viscoelasticity. *Nat. Mater.* **12**, 932–937 (2013).
45. X. Li, F. Luo, T. L. Sun, K. Cui, R. Watanabe, T. Nakajima, J. P. Gong, Effect of salt on dynamic mechanical behaviors of polyampholyte hydrogels. *Macromolecules* **56**, 535–544 (2023).
46. K. Cui, J. P. Gong, How double dynamics affects the large deformation and fracture behaviors of soft materials. *J. Rheol.* **66**, 1093–1111 (2022).
47. X. Li, J. P. Gong, Role of dynamic bonds on fatigue threshold of tough hydrogels. *Proc. Natl. Acad. Sci. U.S.A.* **119**, e2200678119 (2022).
48. A. Eisenberg, B. Hird, R. Moore, A new multiplet-cluster model for the morphology of random ionomers. *Macromolecules* **23**, 4098–4107 (1990).
49. X. Li, K. Cui, T. L. Sun, L. Meng, C. Yu, L. Li, C. Creton, T. Kurokawa, J. P. Gong, Mesoscale bicontinuous networks in self-healing hydrogels delay fatigue fracture. *Proc. Natl. Acad. Sci. U.S.A.* **117**, 7606–7612 (2020).
50. X. Li, K. Cui, T. Kurokawa, Y. N. Ye, T. L. Sun, C. Yu, C. Creton, J. P. Gong, Effect of mesoscale phase contrast on fatigue-delaying behavior of self-healing hydrogels. *Sci. Adv.* **7**, eabe8210 (2021).
51. K. Cui, T. L. Sun, X. Liang, K. Nakajima, Y. N. Ye, L. Chen, T. Kurokawa, J. P. Gong, Multiscale energy dissipation mechanism in tough and self-healing hydrogels. *Phys. Rev. Lett.* **121**, 185501 (2018).
52. K. Häkkinen, M. Alen, M. Kallinen, R. Newton, W. Kraemer, Neuromuscular adaptation during prolonged strength training, detraining and re-strength-training in middle-aged and elderly people. *Eur. J. Appl. Physiol.* **83**, 51–62 (2000).
53. G. Gavronski, A. Veraksits, E. Vasar, J. Maaroos, Evaluation of viscoelastic parameters of the skeletal muscles in junior triathletes. *Physiol. Meas.* **28**, 625–637 (2007).
54. R. Bai, Q. Yang, J. Tang, X. P. Morelle, J. Vlassak, Z. Suo, Fatigue fracture of tough hydrogels. *Extreme Mech. Lett.* **15**, 91–96 (2017).
55. L. Chen, T. L. Sun, K. Cui, D. R. King, T. Kurokawa, Y. Saruwatari, J. P. Gong, Facile synthesis of novel elastomers with tunable dynamics for toughness, self-healing and adhesion. *J. Mater. Chem. A* **7**, 17334–17344 (2019).
56. J. P. Gong, Why are double network hydrogels so tough? *Soft Matter* **6**, 2583 (2010).
57. T. Nakajima, H. Furukawa, Y. Tanaka, T. Kurokawa, Y. Osada, J. P. Gong, True chemical structure of double network hydrogels. *Macromolecules* **42**, 2184–2189 (2009).
58. J. P. Gong, Y. Katsuyama, T. Kurokawa, Y. Osada, Double-network hydrogels with extremely high mechanical strength. *Adv. Mater.* **15**, 1155–1158 (2003).
59. A. J. Cunanan, B. H. DeWeese, J. P. Wagle, K. M. Carroll, R. Sausaman, W. G. Hornsby, G. G. Haff, N. T. Triplett, K. C. Pierce, M. H. Stone, The general adaptation syndrome: A foundation for the concept of periodization. *Sports Med.* **48**, 787–797 (2018).
60. A. Bandyopadhyay, I. Bhattacharjee, P. Sousana, Physiological perspective of endurance overtraining—A comprehensive update. *Al Ameen J. Med. Sci.* **5**, 7–20 (2012).
61. B. R. Freedman, J. J. Sarver, M. R. Buckley, P. B. Voleti, L. J. Soslowsky, Biomechanical and structural response of healing Achilles tendon to fatigue loading following acute injury. *J. Biomech.* **47**, 2028–2034 (2014).
62. G. Lake, A. Thomas, The strength of highly elastic materials. *Proc. R. Soc. Lond. A Math. Phys. Sci.* **300**, 108–119 (1967).
63. S. Mzabi, D. Berghezan, S. Roux, F. Hild, C. Creton, A critical local energy release rate criterion for fatigue fracture of elastomers. *J Polym. Sci. B* **49**, 1518–1524 (2011).
64. A. B. Ihsan, T. L. Sun, T. Kurokawa, S. N. Karobi, T. Nakajima, T. Nonoyama, C. K. Roy, F. Luo, J. P. Gong, Self-healing behaviors of tough polyampholyte hydrogels. *Macromolecules* **49**, 4245–4252 (2016).
65. A. B. Ihsan, T. L. Sun, S. Kuroda, M. A. Haque, T. Kurokawa, T. Nakajima, J. P. Gong, A phase diagram of neutral polyampholyte–From solution to tough hydrogel. *J. Mater. Chem. B* **1**, 4555–4562 (2013).
66. K. Cui, Y. N. Ye, T. L. Sun, C. Yu, X. Li, T. Kurokawa, J. P. Gong, Phase separation behavior in tough and self-healing polyampholyte hydrogels. *Macromolecules* **53**, 5116–5126 (2020).
67. F. Luo, T. L. Sun, T. Nakajima, T. Kurokawa, Y. Zhao, A. B. Ihsan, H. L. Guo, X. F. Li, J. P. Gong, Crack blunting and advancing behaviors of tough and self-healing polyampholyte hydrogel. *Macromolecules* **47**, 6037–6046 (2014).
68. H. F. Brinson, L. C. Brinson, in *Polymer Engineering Science and Viscoelasticity* (Springer, 2008), pp. 99–157.
69. S. Park, R. Schapery, Methods of interconversion between linear viscoelastic material functions. Part I—A numerical method based on Prony series. *Int. J. Solids Struct.* **36**, 1653–1675 (1999).
70. E. M. Zanetti, M. Perrini, C. Bignardi, A. L. Audenino, Bladder tissue passive response to monotonic and cyclic loading. *Biorheology* **49**, 49–63 (2012).
71. C.-Y. Hui, B. Zhu, R. Long, Steady state crack growth in viscoelastic solids: A comparative study. *J. Mech. Phys. Solids* **159**, 104748 (2022).
72. J. Guo, M. Liu, A. T. Zehnder, J. Zhao, T. Narita, C. Creton, C.-Y. Hui, Fracture mechanics of a self-healing hydrogel with covalent and physical crosslinks: A numerical study. *J. Mech. Phys. Solids* **120**, 79–95 (2018).
73. M. M. Fitzgerald, K. Bootsma, J. A. Berberich, J. L. Sparks, Tunable stress relaxation behavior of an alginate-polyacrylamide hydrogel: Comparison with muscle tissue. *Biomacromolecules* **16**, 1497–1505 (2015).


**Acknowledgments:** We thank L. Chen (Southwest University) for discussion and providing the SAXS data of PPEA elastomer. The SAXS experiments were performed at the NCPSS BL19U2 beam line at Shanghai Synchrotron Radiation Facility (SSRF), China. The Hefei Puliang Technology Co. Ltd. is appreciated for providing the tensile machine with well-controlled humidity and temperature for time-resolved SAXS measurement. **Funding:** This work was supported by JSPS KAKENHI, grant numbers JP22H04968 (J.P.G. and T.N.), JP22K21342 (J.P.G. and T.N.), JP22K20521 (X.L.), and JP23K13796 (X.L.); and by Hokkaido University SOUSEI Support Program for Young Researchers in FY 2022 (X.L.). **Author contributions:** Conceptualization: X.L. and J.P.G. Methodology: X.L. and K.C. Investigation: X.L., K.C., Y.Z., Y.N.Y., and C.Y. Supervision: J. P.G. Writing—original draft: X.L. and J.P.G. Writing—review and editing: X.L., K.C., Y.Z., Y.N.Y., C. Y., W.Y., T.N., and J.P.G. **Competing interests:** The authors declare that they have no competing interests. **Data and materials availability:** All data needed to evaluate the conclusions in the paper are present in the paper and/or the Supplementary Materials.

Submitted 11 July 2023
Accepted 20 November 2023
Published 20 December 2023
10.1126/sciadv.adj6856